A Bidirectional LLC Resonant Converter With Automatic Forward and Backward Mode Transition

Tianyang Jiang, Junming Zhang, *Senior Member, IEEE*, Xinke Wu, *Member, IEEE*, Kuang Sheng, *Senior Member, IEEE*, and Yousheng Wang

***Abstract*—This paper proposes an improved bidirectional LLC resonant topology with a new control scheme. All the switches in the proposed topology can achieve soft switching. Compared with traditional isolated bidirectional dc–dc converters such as dual active bridge converter, the reverse energy and turn-off loss are reduced dramatically, and the conversion efficiency can be much improved. With the proposed new control scheme, the power flow direction and output power of the proposed converter can be changed automatically and continuously, which is attractive for energy storage systems to balance the energy and to keep the dc-bus voltage constant. Performance of the proposed circuit is validated by the experimental results from a 1-kW prototype. Over 97% efficiency is achieved at full load condition based on the prototype.**

***Index Terms*—Bidirectional, energy storage system (ESS), high efficiency, LLC, resonant converter.**

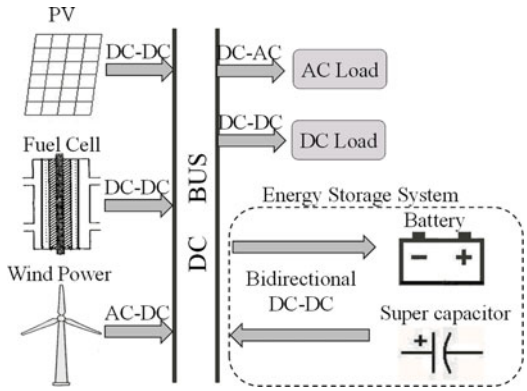

Fig. 1. Typical DG system with ESSs.

I. Introduction

As energy saving and environment protection become more and more important, lots of research efforts have been carried out in order to utilize the energy in a clean and efficient way. The renewable energy resources, such as photovoltaic (PV) and wind power, are the most promising ways for clean electric power generation. However, the intermittent nature of these resources introduces issues like system stability, reliability, and power quality. Energy storage systems (ESSs) are required to deal with such intermittent outages for grid-tied and offgrid applications [1]–[3]. Batteries and super capacitors are the most popular energy storage components considering the price and performance. Fig. 1 shows a typical distributed generation (DG) system with renewable energy resources and ESSs. The ESSs should have bidirectional power flow capability to store the excess energy generated by renewable resources, and release it when the renewable energy is not sufficient or during peak times of energy consumption [4]–[6]. So, the bidirectional dc–dc converter is a key component in ESSs to enable the bidirectional power flow.

Manuscript received October 17, 2013; revised December 31, 2013; accepted February 6, 2014. Date of publication February 20, 2014; date of current version October 7, 2014. This work was supported by the National Nature Science Foundation of China under Grants 51277161, 51007081, and the National High Technology Research and Development Program of China 863 Program 2011AA050402. Recommended for publication by Associate Editor S. Choi.

The authors are with the College of Electrical Engineering, Zhejiang University, Hangzhou 310027, China (e-mail: jiangtianyangtc@zju.edu.cn; zhangjm@zju.edu.cn; wuxinke@zju.edu.cn; shengk@zju.edu.cn; eewangys@163.com).

Color versions of one or more of the figures in this paper are available online at http://ieeexplore.ieee.org.

Digital Object Identifier 10.1109/TPEL.2014.2307329

Generally, bidirectional dc–dc converters for ESSs should have high-power density, high efficiency, and high reliability. Various bidirectional dc–dc topologies have been proposed and studied in the past decades [7]–[27]. For safety consideration, the galvanic isolation is usually required. Among these isolated topologies, the dual active bridge (DAB) converter has attracted lots of research interests due to its simple structure, wide range soft switching capability, and high efficiency [14]–[21]. The DAB converter has two bridge type switches in each side of the transformer, and the phase shift angle between the primary side switches and the secondary side switches determines the power flow direction and its output power [14], [15]. However, it suffers from high reverse energy and high turn-off power loss which deteriorate the overall efficiency [21]–[25]. A lot of methods have been proposed to further improve its efficiency and performance. An improved DAB topology with reduced reverse energy and simple control scheme was proposed in [21], but the topology lost the bidirectional power flow capability. Several control methods with two or more phase shift angles as control variables were proposed to minimize the reverse energy in [22]–[25], but the control methods were a little bit complex and the turn-off loss was still high.

The turn-off power loss is related to the turn-off current, which can be reduced by operating the DAB topology in resonant mode with an extra resonant capacitor, i.e., dual bridge series resonant converter [26], [27]. However, it can only operate under buck mode which is not suitable for wide input/output range applications like ESSs. A new bidirectional SRC for wide voltage range application with clamped capacitor was studied in [28], but the topology itself is complex due to the complex auxiliary circuits.

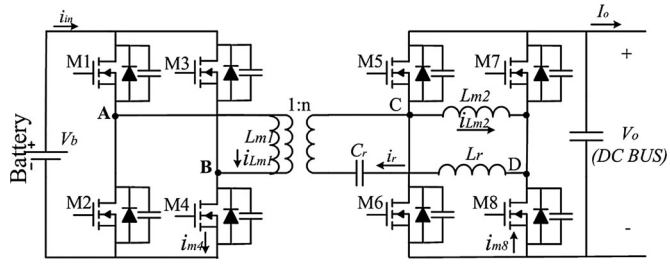

Fig. 2. Proposed bidirectional LLC resonant converter.

Among the resonant converters, the LLC resonant converter has superior performance compared to the series resonant converter (SRC), especially for buck/boost operation capability, narrow switching frequency variation range, and higher efficiency [29]–[32]. Most of the researches on LLC resonant converter are focused on unidirectional dc–dc applications, and very little research work on bidirectional LLC resonant converter was reported in the literature. A bidirectional LLC resonant topology for vehicular applications was proposed in [33]. The topology was still a traditional SRC during backward operation, which is not preferred for wide voltage range application. In [34], a bidirectional CLLC resonant converter with two resonant tanks in the transformer primary side and secondary side, respectively, was proposed. The extra resonant tank increased both the cost and volume of the converter, and the voltage gain was reduced compared with the traditional LLC converter. Furthermore, it uses the dead-band control and the output voltage cannot be regulated continuously. And the current in the output side has to flow through the body diodes of the switches which may cause high conduction loss.

This paper proposes a new bidirectional LLC resonant converter with a new control scheme for ESSs applications. The circuit diagram is shown in Fig. 2. The detailed operating principle is presented in Section II. The theoretical analysis of the proposed topology is given in Section III. Section IV presents the experimental results from a 1-kW prototype with 75 V–130 V input and 400-V output.

II. Principle of Operation

The proposed bidirectional LLC resonant converter is shown in Fig. 2. The energy storage element is in the transformer primary side and the dc bus is in the secondary side. For bidirectional power flow, two active bridges are adopted in the proposed topology. It should be noted that a half-bridge structure can also be used. An extra inductor L_{m2} is added between point C and point D.

In this paper, the forward mode means the battery delivers energy to the dc bus, which is a discharging mode. And the backward mode is a charging mode. The voltage gain G is the ratio of dc-bus voltage referred to the primary side to the battery voltage, which is equal to V_o/nV_b, where n is the transformer turns ratio as shown in Fig. 2.

For $G \geq 1$, the auxiliary inductor L_{m2}, resonant inductor L_r and resonant capacitor C_r form the LLC resonant tank, and the transformer magnetizing inductor L_{m1} is used to help to achieve ZVS for MOSFETs in the primary side. For $G < 1$, the resonant inductor L_r, resonant capacitor C_r and transformer magnetizing inductor L_{m1} form the LLC resonant tank, and the auxiliary inductor L_{m2} is used to help to achieve ZVS for secondary side switches. If L_{m2} (referred to the primary side) is equal to L_{m1}, the parameters of resonant tank are exactly the same, and the converter is symmetrical, which means the operation is also the same.

The control scheme is very important to achieve the desired characteristics of the proposed topology. The most straightforward control scheme is turning ON and OFF the primary side switches and secondary side switches with same switching frequency [35]. The diagonal switches M1/M4 and M2/M3 in the input bridge are switching with 50% duty cycle and complementarily without considering the dead time. The gate drive signals for M5/M8 and M6/M7 in the output bridge are the same as those for M1/ M4 and M2/M3, respectively, which can be regarded as the synchronous control. The switching frequency is used to control output power as traditional LLC resonant converter. Thus, the high conduction loss and poor reverse recovery problem of MOSFET body diodes in the output side can be avoided. And the current in the output side is always in continuous conduction mode (CCM) even when the switching frequency is below the resonant frequency, which is different from traditional unidirectional LLC converter. Moreover, the output characteristic such as voltage gain is also different.

The voltage gain of traditional unidirectional LLC resonant converter with diode rectifier in the ouput side is given in (1) [36]

$$G = \frac{1}{\sqrt{[1+\frac{1}{k}(1-\frac{1}{x^2})]^2 + Q^2(x-\frac{1}{x})^2}} \tag{1}$$

where $k = L_{m2}/L_r$ is the inductance ratio, $Z_r = \sqrt{L_r/C_r}$ is the characteristic impedance, $f_r = 1/2\pi\sqrt{L_r \cdot C_r}$ is the resonant frequency, f_s is the switching frequency, $x = f_s/f_r$ is the normalized switching frequency, R_o is the equivalent dc-load resistance, and $Q = \pi^2 Z_r/8n^2 R_o$ is the quality factor.

The voltage gain of the proposed bidirectional LLC converter with the synchronous control method is given in (2) [35]. The output current is always in CCM with the synchronous control method when $f_s < f_r$. And the equivalent output current has a phase angle φ leading to the output voltage. Therefore, the equivalent load in the fundamental harmonic approximation analysis model is complex impedance instead of a resistor. And the phase angle φ can be used to represent the impedance angle of the equivalent output impedance. When the switching frequency is above or equal to the resonant frequency, the operation with synchronous control method is the same as a traditional LLC resonant converter with diode rectifier, and the equivalent load can also be seen as a resistor, so φ is 0 when $f_s \geq f_r$ [35]

$$G = \frac{1}{\sqrt{\left(\frac{kx^2+x^2-1}{kx^2}\right)^2 - 2Q\tan\varphi\frac{(x^2-1)(kx^2+x^2-1)}{kx^3} + \frac{Q^2(x^2-1)^2}{\cos\varphi^2 x^2}}}. \tag{2}$$

A plot of these two voltage gains is shown in Fig. 3. It is seen that the voltage gain of the proposed topology with the

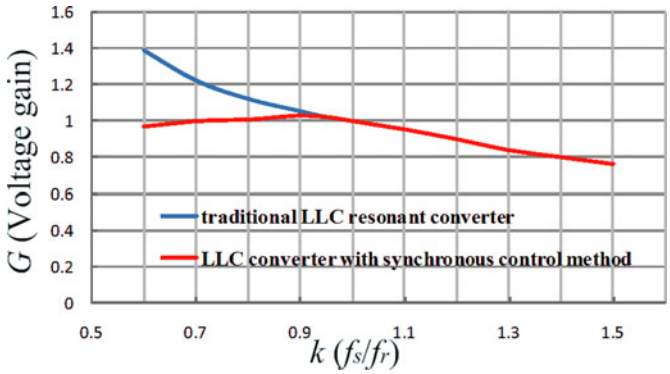

Fig. 3. Voltage gain with $k = 4$, $Q = 0.4$.

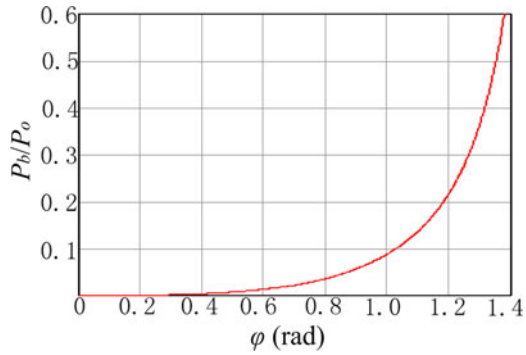

Fig. 4. Ratio of the reverse power to the output power with the synchronous control scheme.

synchronous control scheme is same as the traditional one when $f_s \geq f_r$, but it is much lower than the traditional one when $f_s < f_r$. Since φ will increase with the decreasing of the switching frequency, the maximum voltage gain is limited due to large reverse power. The reverse energy exists for the output voltage and output current are not in phase, which means part of the energy is transferred back and forth between the output side and the input side, so the conduction loss will increase. For simplicity, the reverse energy per unit time can also be represented by the reverse power. The ratio of reverse power P_b to the output power P_o is given in (3), which is shown in Fig. 4 [35]. It is seen in Fig. 4 that the reverse power will also increase when φ increases, which means more energy is reversed from the output side in a switching period, and it will result in higher conduction loss

$$\frac{Pb}{Po} = \frac{\int_{\frac{(\pi-\varphi)}{2\pi}T_s}^{\frac{T_s}{2}} [v_{CD1}(t) \bullet i_{CD1}(t)]dt}{\int_0^{\frac{T_s}{2}} [v_{CD1}(t) \bullet i_{CD1}(t)]dt} = \frac{\sin\varphi - \varphi\cos\varphi}{2\pi\cos\varphi}. \tag{3}$$

From Fig. 4, it is clear that the reverse energy will become very large when the switching frequency keeps decreasing in order to get a high voltage gain. And the high reverse energy finally limits the voltage gain. The dc-bus voltage cannot maintain when the battery voltage drops during discharging mode due to limited voltage gain. So, the synchronous control method is not suitable for bidirectional LLC converter need wide operating voltage range.

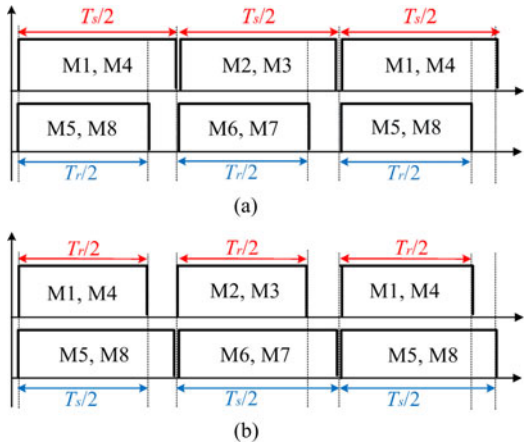

Fig. 5. Gate drive signals of the proposed control schemes. (a) $G \geq 1$. (b) $G < 1$.

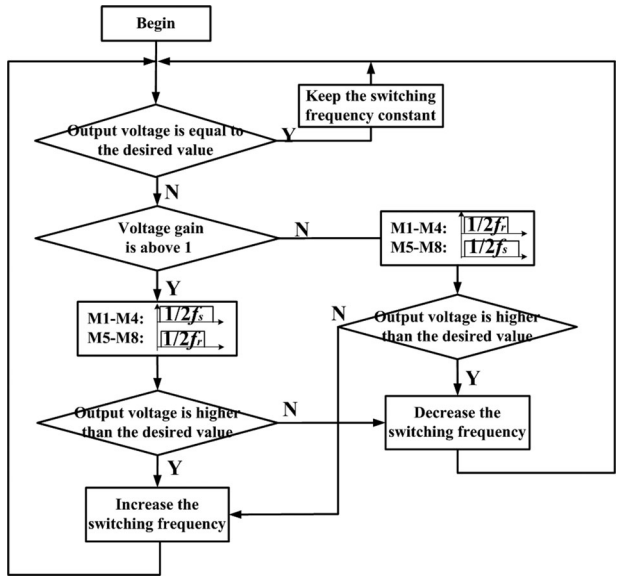

Fig. 6. Output regulating method using the proposed control scheme.

Generally, for a typical DG system, the dc-bus voltage should be regulated to a constant value. And the converter should automatically switch between the discharging mode and charging mode according to the energy consumed by the load and generated by the generators. Also, it is preferred that the bidirectional dc–dc convetrer can operate in buck/boost mode due to the large terminal voltage variation of the ESS.

To meet these requirements, this paper proposes a new control scheme for the proposed bidirectional LLC topology. With the proposed control method, the converter is always operating below the resonant frequency f_r. All the MOSFETs in the converter are switching with same frequency, but the pulse width of gate drive signals for primary side MOSFETs and secondary side MOSFETs are different according to the voltage gain G.

The gate drive signals with different voltage gain are shown in Fig. 5, in which T_r is the resonant period formed by L_r, C_r, and T_s is the switching period, and Fig. 6 shows the flow chart of how to regulated the ouput power with different voltage gain. When the output voltage is deviated from the desired value, if

the required voltage gain is above 1, the on time of secondary side MOSFETs is fixed to half the resonant period $T_r/2$ as shown in Fig. 5(a). The switching frequency increases when the output voltage is higher than the desired vluae and decreases when the output voltage is lower than the desired value. If the desired voltage gain is below 1, the maximum on time of primary side MOSFETs is fixed to half the resonant period as shown in Fig. 5(b), and the switching frequency decreases when the output voltage is higher than the desired value and increases when the output voltage is lower than the desired value. The voltage gain, output power as well as the power flow direction can be regulated by changing the switching frequency in this way. With the proposed control method, the reverse energy can be used to achieve $G < 1$ when the switching frequency is below f_r, so it is not necessary to increase the switching frequency above the resonant frequency.

The control law is implemented by a DSP TMS320F28335 from TI. The DSP samples the output voltage by its A/D input and controls the output voltage by changing the register value for digital pulse width modulation period, which changes the switching frequency. Thus, the output voltage can keep constant based on the flow chat shown in Fig. 6.

Figs. 7 and 8 show steady-state waveforms for $G \geq 1$ and $G < 1$,respectively. When the switching frequency is equal to the resonant frequency f_r, the pulse width of gate drive signals for all the switches are the same and the voltage gain is equal to 1. In Figs. 7 and 8, V_{Cr} is the resonant capacitor voltage, i_r is the resonant inductor current, i'_{Lm1} is the transformer magnetizing current i_{Lm1} referred to the secondary side, i_{Lm2} is the current through auxiliary inductor L_{m2}, i_{m4} is the current through MOSFET M4, and i_{m8} is the current through MOSFET M8. In Figs. 7(c) and 8(c), φ is the phase difference angle between the equivalent output current and the equivalent output voltage as described previously. The reference directions for these voltages and currents are shown in Fig. 2. The relationships of the currents in a half switching cycle are given in (4) and (5)

$$i_{m8} = i_r - i_{Lm2} \tag{4}$$

$$\frac{i_{m4}}{n} = i_r + i_{Lm1}{}' \tag{5}$$

where n is the transformer turns ratio.

For $G \geq 1$, the output power will increase by decreasing the switching frequency, and vice versa. This is reasonable since the on time of secondary side MOSFETs is half the resonant period, and the operation is similar to a diode rectifier in a traditional unidirectional LLC resonant converter. By increasing the switching frequency, the output power will decrease. At a certain critical switching frequency, the average output current will be zero. And the output current will be negative if the switching frequency increases further. Then, the converter is automatically operating in backward mode (charging mode) with same voltage gain. Once the dc-bus voltage is higher than the set point due to excess energy from the generators, the excess energy will automatically flow from the dc bus to the battery until the dc-bus voltage goes back to the initial value again.

For $G < 1$, the switching frequency should decrease to reduce the energy delivered to the output, and vice versa. The reason is that a decreased switching frequency leads to an increased reverse energy and the output power will decrease correspondingly. There is also a critical switching frequency for a given voltage gain G, at which the average output current is zero. If the switching frequency is below this critical value, the converter will operate in backward mode.

The operation of the proposed topology along with the control scheme is symmetrical for forward mode with $G > 1$ and backward mode with $G < 1$ by simply swapping the input and output side. So, only the operating principle for $G > 1$ is analyzed in this paper.

A. $i_o > 0$

When energy generated in the distributed system is not sufficient, the ESS (battery) is discharged to deliver energy to the load, so the output current of the bidirectional converter is positive. In this discharging mode, the auxiliary inductor L_{m2} is part of the LLC resonant tank and the transformer magnetizing inductor L_{m1} helps to achieve ZVS for M1 to M4. This operating mode is similar to the traditional unidirectional LLC resonant converter when $f_s < f_r$, and there are three operating modes in a half switching cycle, which are shown in Fig. 9(a), (b), and (d).

Mode 1 $(t_0$–$t_1)$: The equivalent circuit of this mode is shown in Fig. 9(a). M1, M4, M5, and M8 turn ON at t_0 with ZVS. The voltage across the auxiliary inductor L_{m2} is equal to V_o, so i_{Lm2} increases linearly. Voltage across the transformer magnetizing inductor L_{m1} is equal to V_b, and its current increases linearly, too. In this mode, L_r resonant with C_r and i_r is always larger than i_{Lm2}. This mode ends when M5 and M8 turn OFF at t_1 when i_r is equal to i_{Lm2}, so M5 and M8 turn OFF with ZCS.

Mode 2 $(t_1$–$t_2)$*:* The equivalent circuit is shown in Fig. 9(b). The output is disconnected from the resonant tank, and energy to the load is supplied by the output capacitor. In this mode, C_r, L_r, and L_{m2} form the resonant tank, so i_{lm2} and i_r are the same. As the resonant period is quite long, i_r will increase very slowly due to large inductance of L_{m2}.

Mode 3 $(t_2$–$t_3)$*:* The equivalent circuit is shown in Fig. 9(d). M1 and M4 turn OFF at t_2. i_r plus i_{Lm1} charge the parasitic capacitors of M1 and M4, and discharge the parasitic capacitors of M2 and M3 until the voltage across M1 and M4 reaches the input voltage, then current in the primary side begins to flow through the body diodes of M2 and M3. Then, current in the secondary side begins to flow through the body diodes of M6 and M7, so they will turn ON with ZVS.

B. $i_o = 0$

When energy generated in distributed system exactly matches the load power, the energy transferred between the battery and the dc bus will be zero. And the steady state waveforms are shown in Fig. 7(b). There are also three operating modes in a half switching cycle, which are shown in Fig. 9(a), (c), and (d).

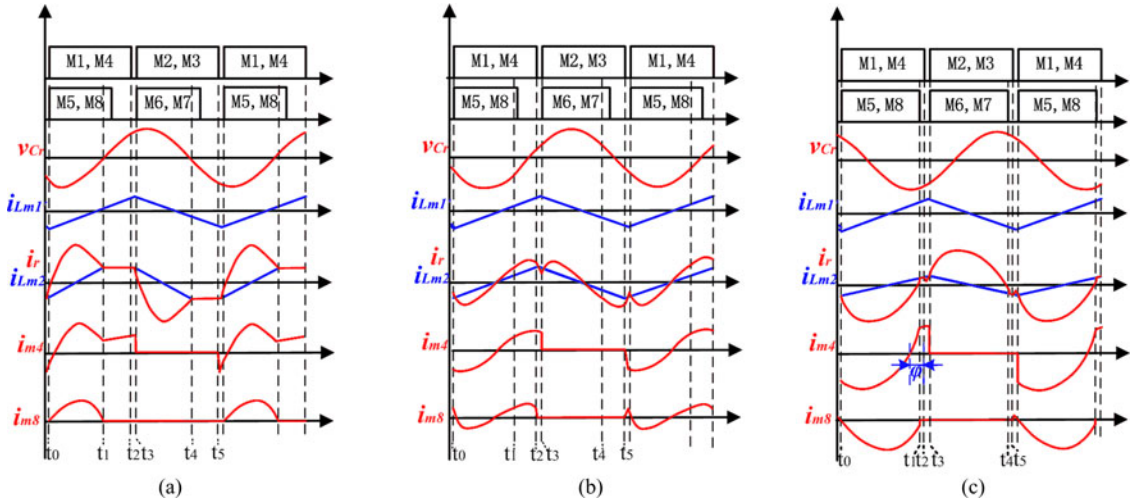

Fig. 7. Steady-state waveforms when $G \geq 1$. (a) $i_o > 0$. (b) $i_o = 0$. (c) $i_o < 0$.

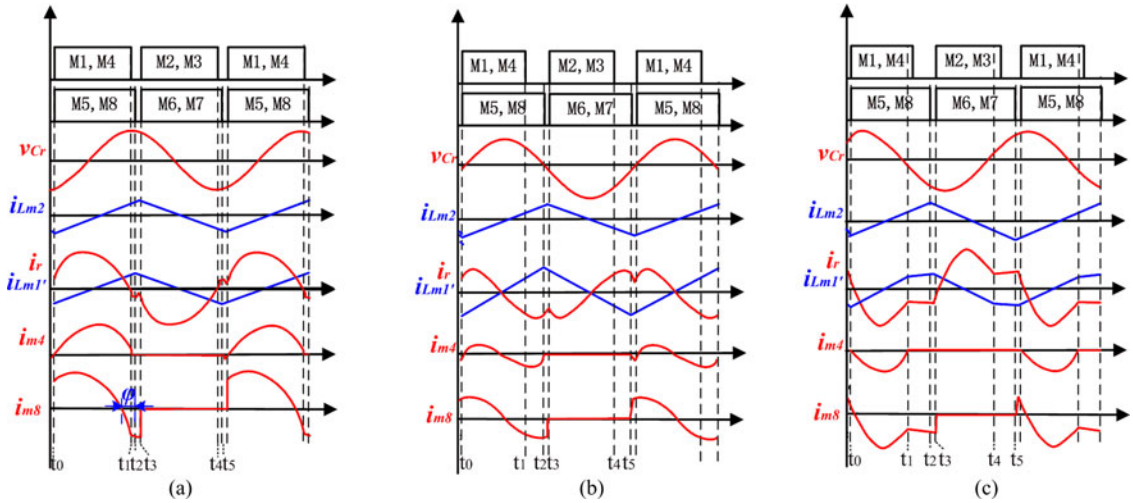

Fig. 8. Steady-state waveforms when $G < 1$. (a) $i_o > 0$. (b) $i_o = 0$. (c) $i_o < 0$.

Mode 1 $(t_0$–$t_1)$: M1 and M4 turn ON with ZVS at t_0. The equivalent circuit of this mode is also shown in Fig. 9(a). The secondary side current is positive at t_o, and then the resonant begins. This mode ends when M5 and M8 turn OFF at t_1, which is also the end of the half resonant cycle.

Mode 2 $(t_1$–$t_2)$: i_r is still larger than i_{Lm2} in this mode, so current in the secondary side will flow through the body diodes of M5 and M8, and the equivalent circuit is shown in Fig. 9(c). This mode ends when M1 and M4 turn OFF at t_2.

Mode 3 $(t_2$–$t_3)$*:* The equivalent circuit is shown in Fig. 9(d). In the primary side, the parasitic capacitors of M2 and M3 are discharged, and the current will flow through their body diodes once the voltage across M1/M4 reaches zero, so M2 and M3 can turn ON with ZVS in the next half switching cycle. In the secondary side, current begins to flow through the body diodes of M6 and M7.

C. $i_o < 0$

When there is excess energy generated by the generators in the distributed system, the feedback loop will increase the switching frequency to reduce the energy from ESS to the load. If the switching frequency is above the critical value, the average output current is negative and the converter automatically operating in backward mode. The steady-state waveforms are shown in Fig. 7(c). There are also three operating modes in a half switching cycle, and the equivalent circuits are the same as those for $i_o > 0$, which are also shown in Fig. 9(a), (b), and (d).

Mode 1 $(t_0$–$t_1)$: The equivalent circuit and operation is the same as that describe in Mode 1 when $i_o > 0$, the difference is that i_r is always lower than i_{Lm2} in this mode. According to (4), the current of M5 and M8 is always negative and energy flows from the secondary side to the primary side. This mode ends when M5 and M8 turn OFF at t_1.

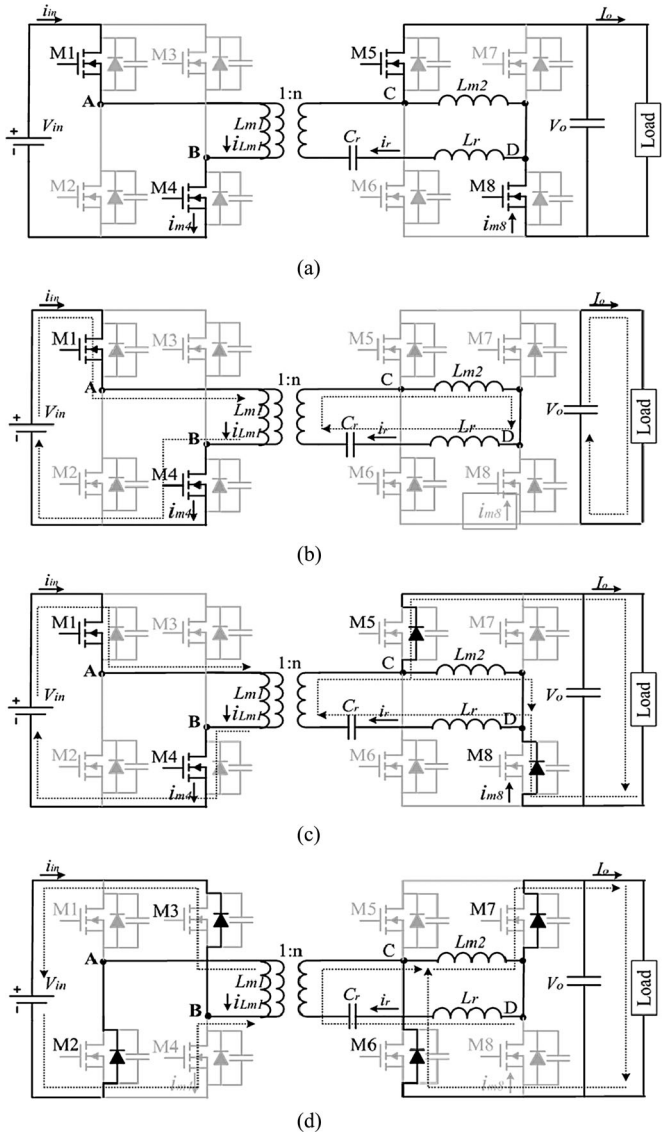

Fig. 9. Operating modes with different voltage gain and output current in half switching cycle.

Mode 2 (t_1–t_2)*:* The equivalent circuit is shown in Fig 9(b). When M5 and M8 turn OFF at t_1, current flows through them is negative, so it will charge the parasitic capacitors of M5/M8 and discharge the parasitic capacitors of M6/M7. When M5 and M8 have turned OFF, L_{m2} will be resonant with L_r and C_r. This mode ends when M1 and M4 turn OFF at t_2.

Mode 3 (t_2–t_3)*:* The voltage across M5/M8 reaches V_o, the body diodes of M6 and M7 conduct, so M6 and M7 will turn ON with ZVS in the next half switching cycle. This mode is almost the same as Mode 3 when $i_o > 0$, and only the current direction is reversed, which will not be repeated here.

According to the analysis of operation mode for $G \geq 1$, it is clear that the converter can operate automatically from forward mode to backward mode. With the proposed gate drive pattern, the switching frequency modulation can be used to control the output power and its direction. The operation of the proposed converter under $G < 1$ is a dual to that with $G \geq 1$, which will not be elaborated here.

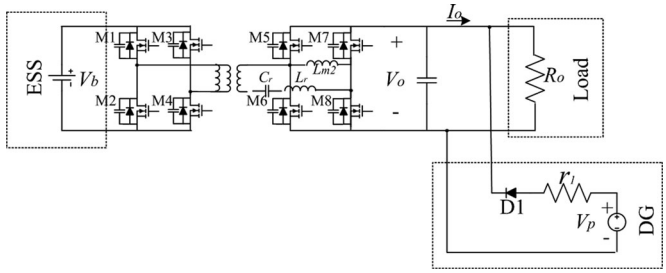

Fig. 10. Simulation model of bidirectional operation.

III. Converter Characteristics Analysis

Since energy generated in DG system like PV or wind power always changes, and the load condition may also vary with time, the bidirectional converter in ESS has to regulate the output power to keep the dc-bus voltage constant. A typical DG system with ESS (battery) is shown in Fig. 10. The proposed bidirectional dc–dc converter is used as the interface between the battery and the dc bus. V_p is the equivalent output voltage of the renewable energy resources, such as PV panels. The resistor r_1 is used to simulate the output characteristics of the renewable energy resources, the cable resistance of dc bus and parasitic resistance. D1 is used to simulate the unidirectional energy flow of the renewable energy resources. V_b is the battery terminal voltage and V_o is the dc-bus voltage which is also the output voltage of the bidirectional dc–dc converter.

A. Voltage Gain G

Due to different control schemes, the characteristic of voltage gain G is different from the traditional unidirectional LLC converter. It will be discussed firstly.

When G is above 1, the operating principle is similar to the traditional LLC resonant converter with the control scheme shown in Fig. 5(a). So, the voltage gain can also be expressed by (1).

When G is below 1 with control scheme shown in Fig. 5(b), though M1 and M4 turn OFF after half the resonant period, the current will still flow through the body diodes of M1 and M4 after they turned OFF since the current through M1/M4 is still negative at t_1. So, the converter is always operating in CCM mode, which is similar to that with synchronous control as analyzed in [35]. And the voltage gain can also be expressed by (2).

The phase shift angle φ between the equivalent output current and voltage given in (2) is a function of switching frequency f_s, the quality factor Q, the equivalent load resistance R_o, and the magnetizing inductor L_{m2}, and the expression is a transcendental equation, so it is not possible to get its theoretical solution. In order to simplify the analysis and get a reasonable engineering design guide, φ is assumed to have quadratic functional relationship with the equivalent switching frequency x ($x = f_s/f_r$), which is given in (6). The assumption is reasonable because φ is 0 when $f_s = f_r$, and φ will increase with the decrease of f_s

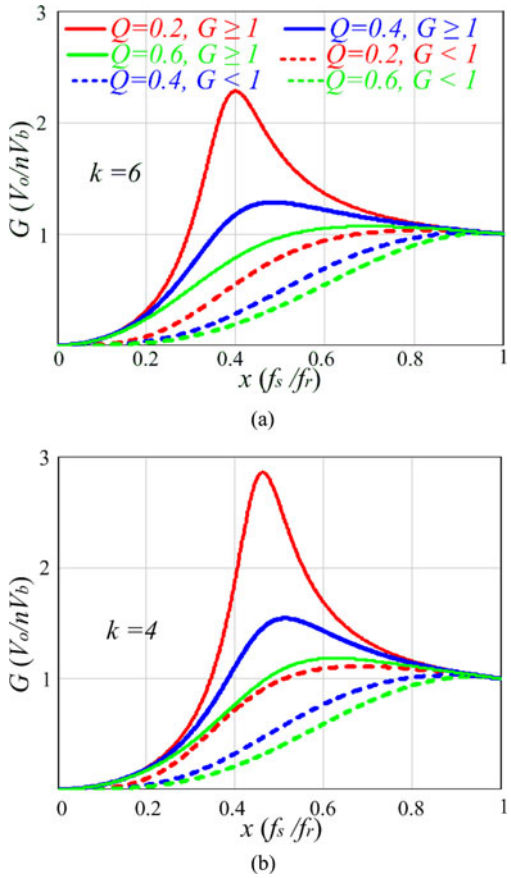

Fig. 11. Voltage gain. (a) $k = 6$. (b) $k = 4$.

and it will not exceed $\pi/2$

$$\varphi = \frac{\pi(1-x^2)}{2}. \tag{6}$$

Taking (6) into (2), the voltage gain is approximately derived as in (7).

Fig. 11(a), (b) show the voltage gain calculated based on (1) and (7) with different quality factor Q and inductance ratio k. The gain curves for $G \geq 1$ and $G < 1$ are shown in solid line and dotted line respectively. It is seen that the voltage gain has two solutions at each switching frequency due to the different gate drive signals.

Since the converter is always operating below the resonant frequency, the reverse energy is used to achieve voltage gain below 1 like synchronous control method. Therefore, for $G < 1$, the reverse energy can also be expressed by (3). With the assumption of phase shift angle given in (6), the ratio of reverse power to output power is a function of normalized switching frequency x, which is given in (8) and is also shown in Fig. 12.

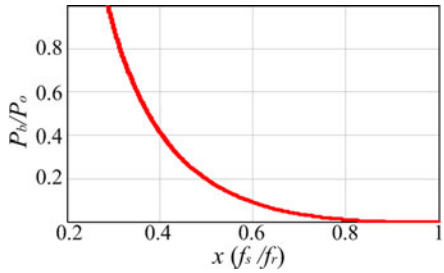

Fig. 12. Ratio of reverse power to output power versus the normalized switching frequency.

To avoid excessive reverse energy, the minimum voltage gain should not be too low in the design

$$\frac{P_b}{P_o} = \frac{\tan[\frac{\pi(1-x^2)}{2}]}{2\pi} - \frac{1-x^2}{4}. \tag{8}$$

B. Soft Switching

It is known from traditional LLC resonant converter, that there is a boundary between the capacitive region (ZCS) and inductive region (ZVS) for the primary side MOSFETs when the switching frequency is below the resonant frequency [31]. Operation in the capacitive region should be avoided for reliable operation. In the proposed topology, the transformer magnetizing current i_{Lm1} also provides extra inductive current, the inductive region will be wider and it is easier to achieve ZVS. For simplicity, the design for traditional LLC resonant converter can be adopted for $G > 1$ of the proposed converter.

For $G < 1$, there is also a boundary between the inductive region and capacitive region. Operation of the primary side switches should always be in ZVS region to avoid the capacitive switching. So, the turn-on current of primary side MOSFETs at t_o shown in Fig. 8 should be negative, and (9) should always be satisfied. The expressions of magnetizing current and resonant current in a half switching cycle are given in (10) and (11), and I_{peak} is the peak value of the equivalent output current, which is derived in (12)

$$i_{m4}(t_o) = n i_r(t_o) + i_{Lm1}(t_o) \leq 0 \tag{9}$$

$$i_{Lm1}(t) = \frac{V_b t}{L_{m1}} - \frac{V_b}{4L_{m1}f_s} \qquad (0 \leq t \leq 1/2f_s) \tag{10}$$

$$i_r(t) = i_{Lm2}(t) + i_{m8}(t) = \frac{V_o t}{L_{m2}} - \frac{V_o}{4L_{m2}f_s} + I_{\text{peak}} \sin(\omega_r \cdot t + \varphi) \quad (0 \leq t \leq 1/2f_s) \tag{11}$$

$$2 \cdot f_s \cdot \int_0^{2/f_s} I_{\text{peak}} \sin(\omega_r \cdot t + \varphi) dt = I_o = \frac{V_o}{R_o} \tag{12}$$

where ω_r is the resonant frequency in rad/s, and $\omega_r = 2\pi f_r$.

$$G = \frac{1}{\sqrt{\left(\frac{kx^2+x^2-1}{kx^2}\right)^2 - 2Q\tan\left[\frac{\pi(1-x^2)}{2}\right]\frac{(x^2-1)(kx^2+x^2-1)}{kx^3} + Q^2\frac{(x^2-1)^2}{\left[\cos\frac{\pi(1-x^2)}{2}\right]^2 x^2}}} \tag{7}$$

Assuming L_{m2} is equal to L_{m1} referred to the secondary side ($L_{m2} = n^2 L_{m1} = L_m$), taking (6), (10), (11), and (12) into (9), the limitation of x to achieve ZVS when $G < 1$ is given in (13). So, once the minimum normalized switching frequency $x_{\min}$ and L_m are designed, they should be taken into (13) to verify the ZVS condition, if (13) is satisfied, soft switching can be achieved in all load condition, else, $x_{\min}$ and L_m should be redesigned

$$x \geq \sqrt{1 - \frac{2\arctan(\frac{2R_o}{\pi L_m f_r})}{\pi}}. \tag{13}$$

C. Output Characteristics

As mentioned previously, the average output current of the converter I_o can be positive or negative depending on the switching frequency. There is a critical switching frequency where I_o reaches zero with a given V_p and V_b. The load R_o shown in Fig. 10 is powered by the bidirectional dc/dc converter and the generators in the system at the same time, which is not the actual load for the dc–dc converter. In backward mode, the equivalent load for the dc–dc converter should be in the battery side. The output side of the dc–dc converter can be simplified to a dc source in series with a resistance r_1 with energy source and sink capability. The equivalent load for the dc–dc converter can be derived based on the output voltage and current.

When $G > 1$ and $I_o \geq 0$, the relationship between the equivalent switching frequency x and output voltage is given in (14), where the equivalent quality factor in the output side $Q_{\mathrm{eq}o}$ is given in (15)

$$\frac{V_p + r_1 I_o}{nV_b} = \frac{1}{\sqrt{[1 + \frac{1}{k}(1 - \frac{1}{x^2})]^2 + Q_{\mathrm{eq}o}^2 (x - \frac{1}{x})^2}} \tag{14}$$

$$Q_{\mathrm{eq}o} = \frac{\pi^2 \sqrt{\frac{L_r}{C_r}} I_o}{8(V_p + r_1 I_o)}. \tag{15}$$

When $G > 1$ and $I_o < 0$, it is a dual to the converter with $G < 1$ and $I_o \geq 0$ since the converter is symmetrical, and the relationship between the equivalent switching frequency x and output voltage is given in (16). Since current is flowing from the generator to the battery, the equivalent quality factor $Q_{\mathrm{eq}b}$ should be calculated in the battery side, and the expression is shown in (17)

$$Q_{\mathrm{eq}b} = \frac{\pi^2 \sqrt{\frac{L_r}{C_r}} (V_p - r_1 I_o) I_o}{8n^2 V_b^2} \tag{17}$$

When L_r, C_r, r_1, k, V_b, and V_p are fixed, the output current I_o versus x can be solved using (14) and (16). Fig. 13(a) shows both the calculated and simulated results of I_o versus x when $G > 1$. And I_o will be zero at the critical switching frequency.

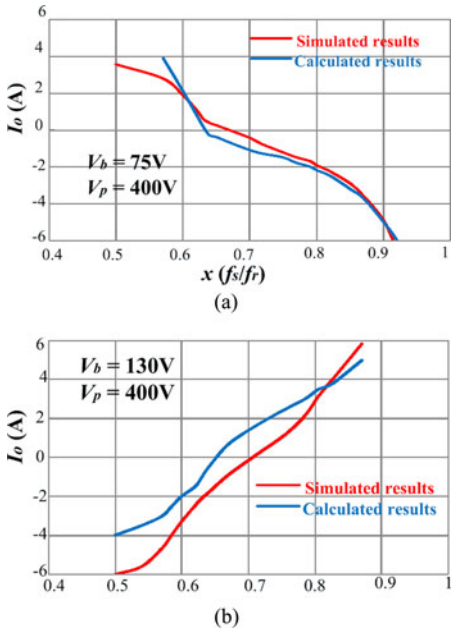

Fig. 13. Output current versus f_s when $L_r = 77\,\mu$H, $C_r = 33$ nF, $r_1 = 10\,\Omega$, $k = 6$. (a) $V_b = 75$ V, $V_p = 400$ V. (b) $V_b = 130$ V, $V_p = 400$ V.

For $G < 1$, the calculation method of I_o versus f_s is similar, and the results are shown in Fig. 13(b). From Fig. 13, it is clear that the converter can automatically operate in forward mode and backward mode by changing the switching frequency. The difference between the calculated one and the simulated one is mainly caused by the assumption in calculating the voltage gain. When $G = 1$, the switching frequency is always equal to the resonant frequency in all the load range in realistic.

IV. Experimental Results

In this paper, a 1-kW prototype with 400-V dc output V_o and 75 V to 130 V dc input V_{in} is designed to verify the analysis given previously. The resonant frequency f_r is 100 kHz. Assuming the nominal dc input voltage is 100 V, so the transformer turns ratio n is set to 4. The maximum voltage gain is 1.3 and the minimum voltage gain is 0.75. The line resistor is 10 Ω.

In order to reduce the conducting loss, the reverse energy for $G < 1$ should be limited. If we want to limit the maximum reverse power below 10% of the maximum output power, the minimum normalized switching frequency $x_{\min}$ is 0.6 according to (8) and Fig. 12. And at that point, the voltage gain reaches its minimum. The inductance ratio and the maximum quality factor $Q_{\max}$ can be designed as a traditional LLC converter with required maximum voltage gain, here $k = 6$ and $Q_{\max} = 0.4$ is adopted. Taking $V_{b\max} = 130$ V, $k = 6$, and $x_{\min} = 0.6$ into (7), the minimum quality factor $Q_{\min} = 0.33$ can be calculated to achieve the desired minimum voltage gain.

$$\frac{nV_b}{V_p - r_1 I_o} = \frac{1}{\sqrt{\left[1 + \frac{1}{k}(1 - \frac{1}{x^2})\right]^2 - 2Q_{\mathrm{eq}b} \tan[\frac{\pi(1-x^2)}{2}](x - \frac{1}{x})[1 + \frac{1}{k}(1 - \frac{1}{x^2})] + Q_{\mathrm{eq}b}^2 \frac{1}{[\cos\frac{\pi(1-x^2)}{2}]^2}(x - \frac{1}{x})^2}} \tag{16}$$

TABLE I
KEY COMPONENTS AND PARAMETERS FOR PROTOTYPE

Parameters	Value	Size/Type	Conductor	Vendor
Resonant capacitor (C_r)	33nF	MKP4J023303C		WIMA
Transformer	n=4 L_{ml}=29uH	EE42/21/15 PC40	Primary side: four 100*Φ0.1mm litz wire in parallel Secondary side: 100*Φ0.1mm litz wire	TDK
Resonant inductor (L_r)	77uH	PQ32/20 PC40	100*Φ0.1mm litz wire	TDK
Auxiliary inductor (L_{m2})	462uH	PQ32/20 PC40	100*Φ0.1mm litz wire	TDK
Primary side MOSFET (M1-M4)	IPP200N15N3G	TO-220		Infineon
Secondary side MOSFET (M5-M8)	IPx65R110CFD	TO-220		Infineon

Considering $Q_{\min}$ and $Q_{\max}$ along with the required resonant frequency, the resonant parameters can be determined, i.e., $C_r = 33$ nF, $L_r = 77$ μH, and $L'_{m1} = L_{m2} = 462$ μH. Taking $x_{\min} = 0.6$, $R_{o\max} = V_o^2 / P_{o\max} = 160$ Ω, and $L_m = 462$ μH into (13), the minimum normalized switching frequency at full load can meet the inequality, so soft switching can be achieved in all load range, and the parameters are well designed. The key components are summarized in Table I. The auxiliary inductor has the same size as the resonant inductor with a PQ32/20 core.

The experimental setup is the same as that shown in Fig. 10. A dc source in series with a resistor and a diode is used to simulate the renewable energy resources (such as PV). The battery is simulated by another dc source with current sink capability.

The steady state waveforms for $G = 1.2$ in forward mode is shown in Fig. 14 and the switching frequency is around 69 kHz. Fig. 14(a) shows the gate drive signal V_{gs4}, current i_{m4} and drain-source voltage V_{ds4} of switch M4. Fig. 14(b) shows the gate drive signal V_{gs8}, current i_{m8} and drain-source voltage V_{ds8} of M8. Fig. 14(c) shows the resonant inductor current i_{Lr} and resonant capacitor voltage V_{Cr}. It is clear that M4 and M8 turn ON with ZVS and M8 turns OFF with ZCS, which match the theoretical waveforms shown in Fig. 7(a) very well. In Fig. 14, there is parasitic oscillation of the drain-source voltage across M8 in the output bridge. Due to DCM operation, all switches in the output bridge are OFF after half the resonant period, and this parasitic ring is caused by the resonant inductor and the parasitic capacitors of the switches in the output bridge, which will not cause any power loss since the energy is very small.

Fig. 15 shows the waveforms when the average output current is around 0, and the switching frequency is about 79 kHz. The theoretical waveforms are shown in Fig. 7(b). Though the turn-off current of M8 in Fig. 15(b) is positive, it drops to zero fast during the dead time. The current slew rate is limited due to the existence of the resonant inductor, and there is almost no reverse recovery current with the fast body diode of MOSFETs.

Fig. 16 shows the waveforms when the average output current is negative for $G = 1.2$. The theoretical waveforms are shown in Fig. 7(c). In the test, the output voltage of the dc source to simulate the generators is set to 450 V, and the converter automatically operates in backward mode. And the output voltage of the dc/dc converter keeps the same due to the voltage drop across resistor r_1. In this mode, the switching frequency is around 92 kHz which is higher than that in Figs. 14 and 15. From Fig. 16(a) and (b), M4 and M8 also turn ON with ZVS. Though current of M8 is negative when it turns OFF as seen in Fig. 16(b), with the help of auxiliary inductor L_{m2}, the turn-off current is quite small.

Figs. 17 and 18 shows the waveforms in forward mode and backward mode when $G < 1$. In Fig. 17, the switching frequency is around 88 kHz. In Fig. 18, the switching frequency is around 73 kHz. The battery voltage is set to 120 V. The theoretical waveforms are shown in Fig. 8. The pulse width of gate drive signals for the primary side MOSFETs are fixed to $1/2f_r$. And the pulse width of gate drive signals for secondary side MOSFETs are $1/2f_s$. As seen in Fig. 17(a), the current through M4 before it turns ON is almost zero, which is not sufficient to achieve ZVS when it turns ON, so it will have certain power loss caused by parasitic capacitance of the MOSFETs. But its current increases very slow due to the resonant inductor and the switching loss especially for the cross-over power loss is still very small. If ZVS is still need, L_m should be further decreased according to (13), which may be not optimized for efficiency under all operation condition.

Fig. 19(a) shows phase angle φ when the voltage gain is equal to 0.8. The calculated results are lower than the accurate value for a quite simple approximation is made in (6), the results will match better if a more complex expression such as $\varphi = \pi\frac{\sqrt{1-x^2}}{2}$ is used, but the calculation will be complicated. Though the approximation has some errors, it shows the trends of φ depended on x. The calculated results can still be used for parameters design, and the measured voltage gain will be a little bit lower than the calculated value as shown in Fig. 19(b).

Fig. 20 shows the dynamic response of bidirectional power flow with G = 1.2, the test setup is also shown in Fig. 10. In stage 1, the converter is steadily operating in forward mode and the battery delivers energy to the load, so I_o is positive. Then, the dc-source voltage steps to 450 V to simulate excessive energy generated by the renewable energy source, the

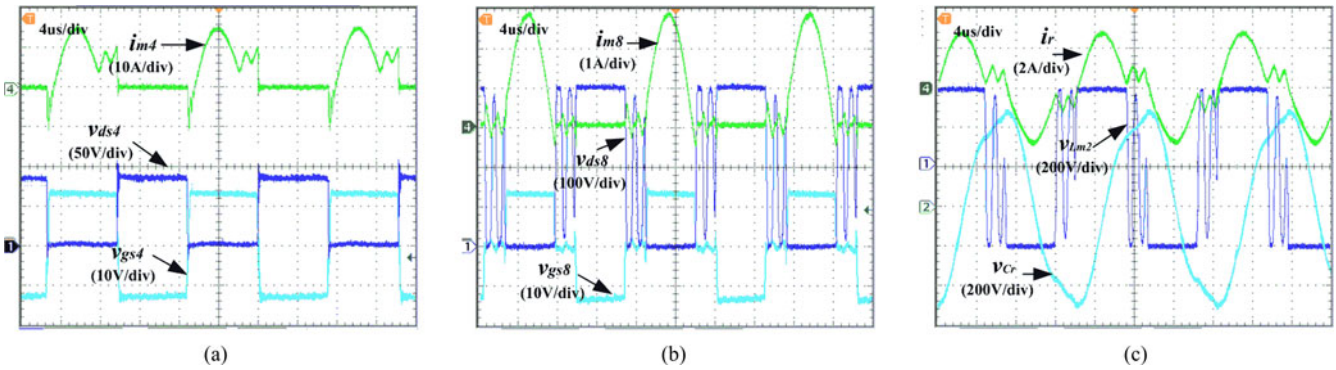

Fig. 14. Experimental waveforms in forward operation @ $G = 1.2$, full load.

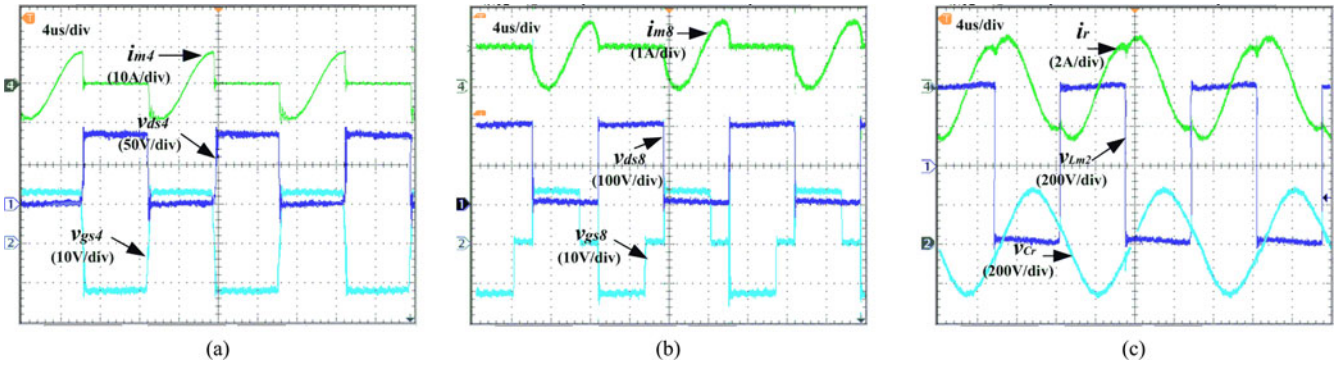

Fig. 15. Experimental waveforms when $i_o \approx 0$ @ $G = 1.2$.

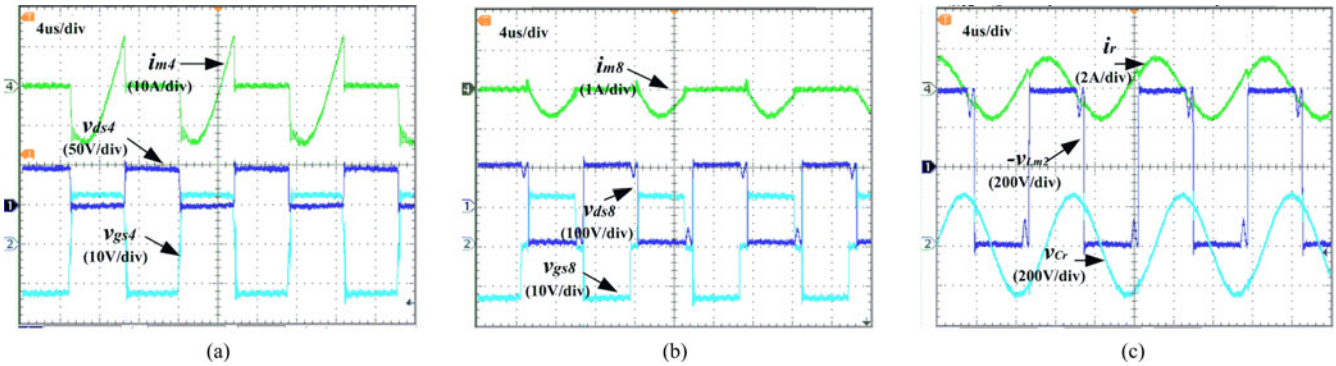

Fig. 16. Waveforms in forward mode when $i_o < 0$ @ $G = 1.2$.

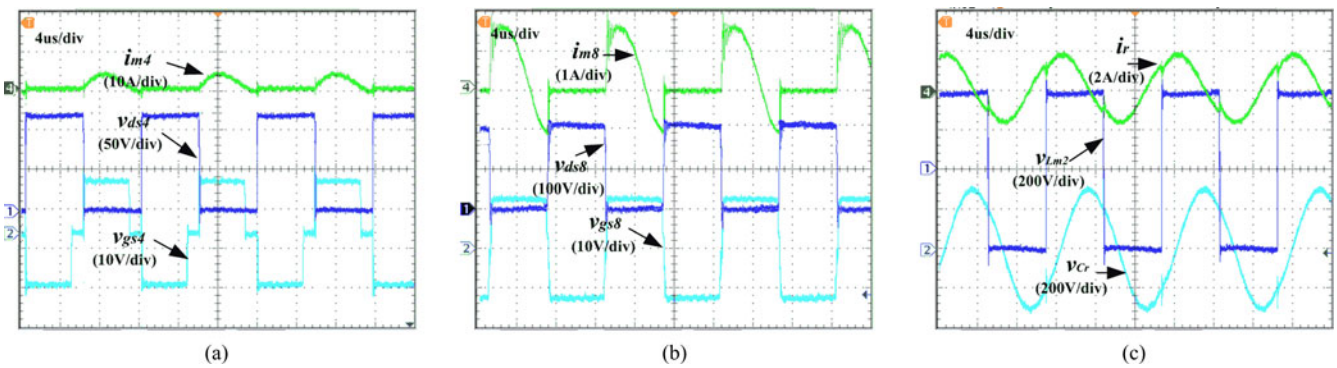

Fig. 17. Waveforms in forward mode @ $G = 0.8$, $P_o = 500$ W.

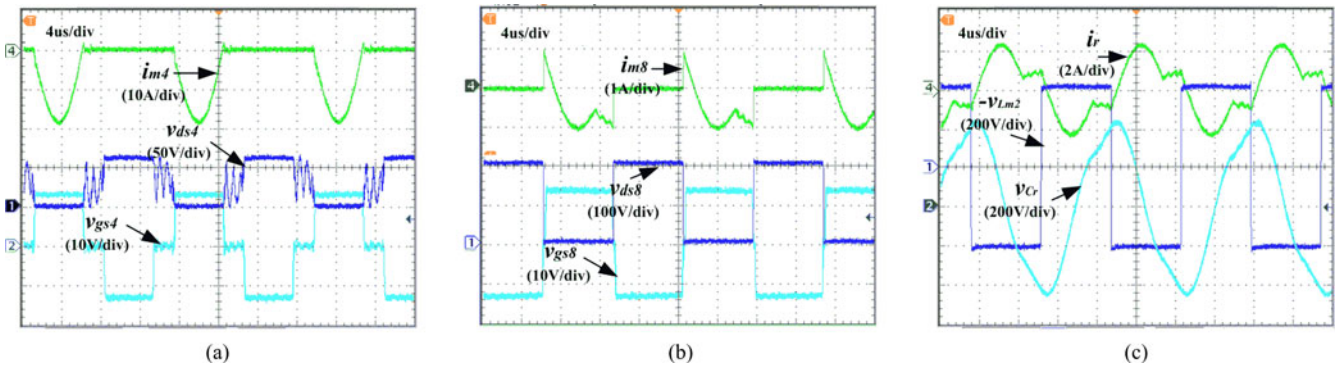

Fig. 18. Waveforms in backward mode @ $G = 0.8$.

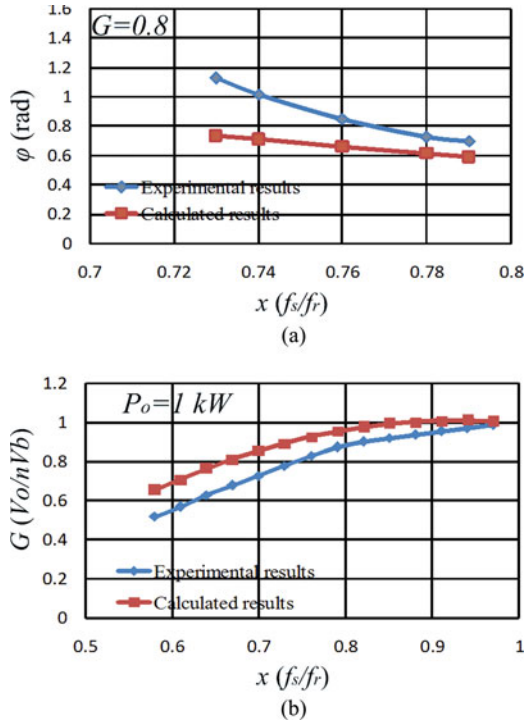

Fig. 19. (a) Comparison of φ when the voltage gain $G = 0.8$. (b) Voltage gain of experimental results and calculated by (7).

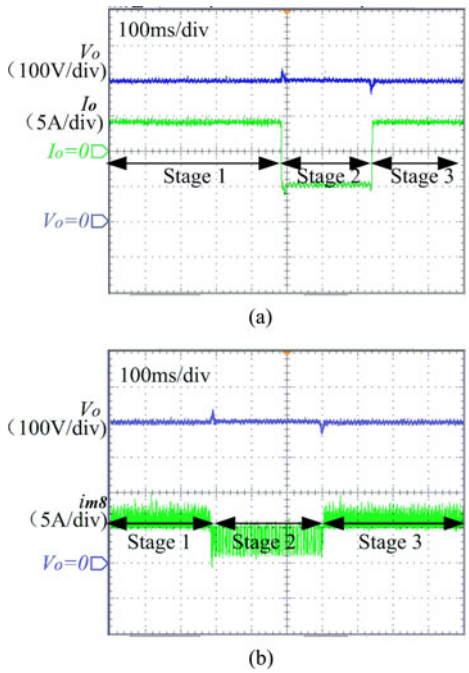

Fig. 20. Dynamic response when voltage gain is above 1. (a) Waveforms of V_o and I_o. (b) Waveforms of V_o and $i_{m\,8}$.

converter changes into backward mode, referred as stage 2 shown in Fig. 20. The output current I_o becomes negative, the converter charges the battery and V_o decreases to its initial value very quickly due to the voltage drop on the resistor r_1. Then, the dc source steps down to 350 V, which is not sufficient to maintain the dc-bus voltage. And the converter operates in forward mode again, which is stage 3 shown in Fig. 20. The output current I_o changes from negative to positive, and V_o keeps constant with a small dip. The battery supplies the energy to the load again. During the transient, there is no output voltage trigger point for the control circuit to switch the converter between the forward mode and backward mode. The regulation is automatically and continuously based on output voltage feedback, which is totally different from the control scheme used in [34].

This dynamic response verifies the effectiveness of the proposed control scheme. The bidirectional LLC resonant converter can automatically operate in forward mode and backward mode using simple switching frequency modulation. Fig. 21 shows the measured output current versus normalized switching frequency in close loop operation. The simulated results with same parameters are also shown for comparison, which matches the experimental results quite well. The differences between the simulated results and experimental results are mainly caused by the tolerance of the component parameters, especially the difference of the resonant frequency.

Fig. 22 shows the measured efficiency of the prototype. For comparison, the traditional DAB converter and the LLC resonant converter using body diode rectifier as described in [34] are also built and tested. The components and parameters design of traditional LLC converter is same with the proposed converter, only the auxiliary inductor is removed and body diodes of the same MOSFETs in the output side are used as output rectifier. The DAB converter is modified from the prototype by simply removing the resonant capacitor, and L_r is replaced by a 50-μH

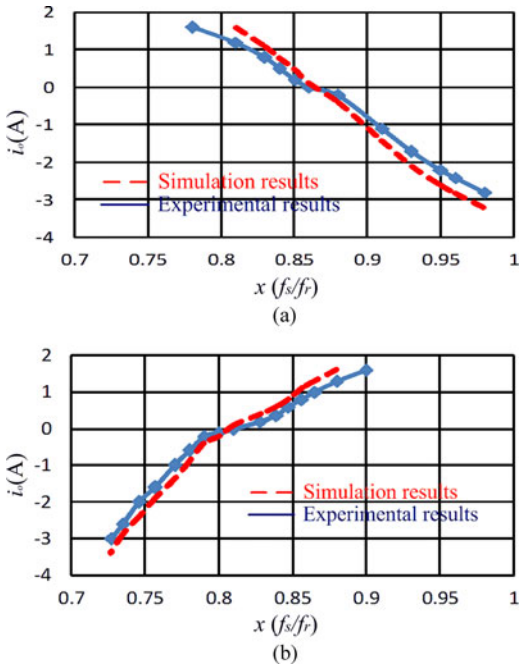

Fig. 21. I_o versus switching frequency. (a) $G = 1.2$. (b) $G = 0.8$.

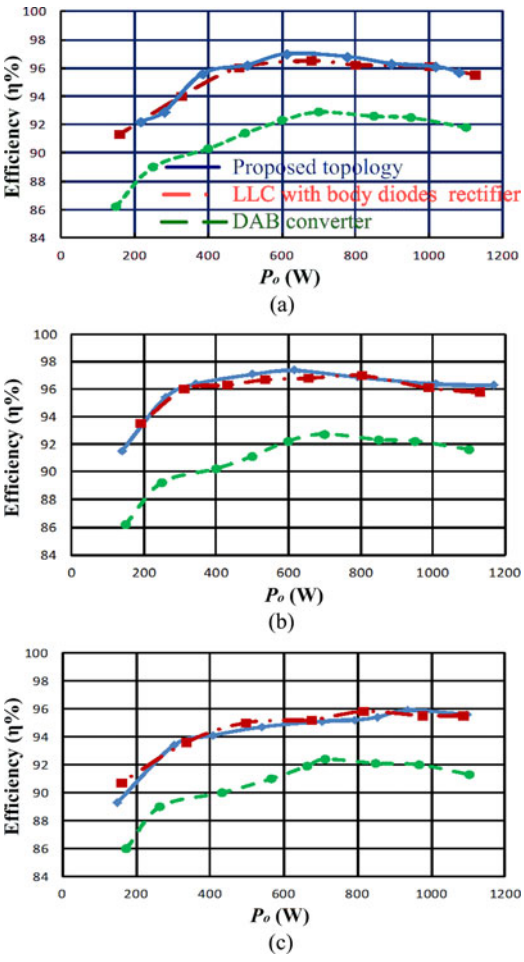

Fig. 22. Measured efficiency in forward operation @ $V_o = 400$ V. (a) $G = 1.2$. (b) $G = 1$. (c) $G = 0.8$.

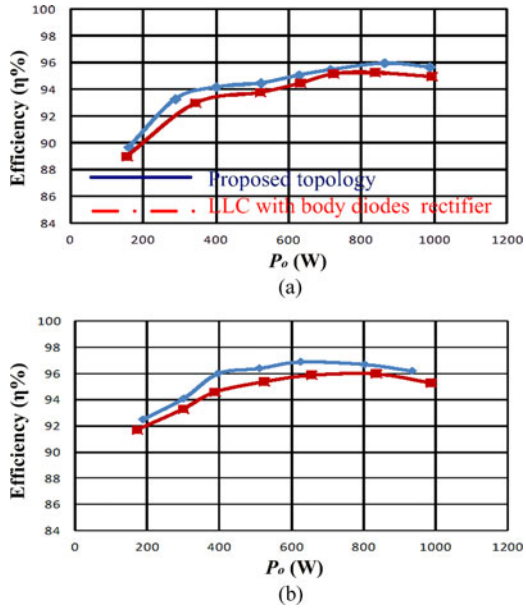

Fig. 23. Measured efficiency in backward operation @ $V_o = 400$ V. (a) $G = 1.2$. (b) $G = 0.8$.

inductor to get same output power. All the other devices keep the same for reasonable comparison. Its seen in Fig. 22 that the efficiency of the proposed topology and traditional LLC converter is very close to each other in forward operation. It is reasonable since the body diode voltage drop of the MOSFET (0.6–0.9 V) is only slightly higher than the voltage drop caused by its channel resistor (about 0.1 Ω). Nevertheless, there is no reverse energy in a traditional LLC converter, so it has less conduction loss compared with the proposed bidirectional LLC converter. Therefore, the total power loss of these two topologies is similar. The comparison of efficiency in the backward mode is shown in Fig. 23. The efficiency of the traditional LLC converter with body diode rectifier is slightly lower, the reason is the equivalent output voltage in backward mode is lower and the body diode voltage drop will cause higher percentage of power loss. The efficiency of the proposed topology is higher than the DAB converter because ZCS is achieved in the output side, so the switching loss is decreased; besides that the reverse energy of the proposed converter is less than the DAB converter which also makes the efficiency of the proposed converter higher. In the proposed topology, the efficiency when $G < 1$ in forward operation and the efficiency when $G > 1$ in backward mode are slightly lower especially when the load is light due to the increased reverse energy.

The main advantages of the proposed topology over a traditional LLC converter are the bidirectional operation and the automatic transition between forward mode and backward mode. By adding an additional inductor, the size and cost will increase. But its known from the analysis before, that the size of the additional inductor is same with the resonant inductor (PQ32/20), so its cost is not significant in the total cost of the prototype. Also, the reactive current generated by the additional inductor could be used to help achieve the soft switching of the secondary side switches, which reduces the switching loss. Its

clear from the efficiency comparison that efficiency is almost the same in forward mode and a little bit higher for the proposed topology in the backward mode. Therefore, the additional inductor also gets some reward in the proposed topology. Compared with the popular analog control circuit for traditional LLC converter, the proposed control method is more suitable for digital implementation, which may not be preferred for low power application.

V. Conclusion

This paper proposes a bidirectional LLC resonant topology along with a new control scheme. An auxiliary inductor is added to make the topology symmetrical in any operating modes. All the switches in the primary side and secondary side turn ON and OFF with the same switching frequency, but the pulse width is different based on the required voltage gain. And the switching frequency is used to regulate the output power and the power flow direction. Therefore, the proposed topology can automatically switch between the forward mode and the backward mode, which is quite attractive for energy storage system applications. The detailed operation principle and topology characteristics are analyzed. Experimental results from 1-kW prototype verify the theoretical analysis. Efficiency above 97% was achieved at full load condition.

References

[1] H. Kakigano, Y. Miura, and T. Ise, "DC micro grid for super high quality distribution-system configuration and control of distributed generations and energy storage devices," in *Proc. IEEE Power Electron., Spec. Conf.*, 2006, pp. 3148–3154.

[2] M. Liserre, T. Sauter, and J. Hung, "Future energy systems: Integrating renewable energy sources into the smart power grid through industrial electronics," *IEEE Trans. Ind. Electron.*, vol. 4, no. 1, pp. 18–37, Mar. 2010.

[3] A. Q. Huang, M. L. Crow, G. T. Heydt, J. P. Zheng, and S. J. Dale, "The future renewable electric energy delivery and management system: The energy internet," *Proc. IEEE*, vol. 99, no. 1, pp. 133–148, Jan. 2011.

[4] S. Inoue and H. Akagi, "A bidirectional dc–dc converter for an energy storage system with galvanic isolation," *IEEE Trans. Power Electron.*, vol. 22, no. 6, pp. 2299–2306, Nov. 2007.

[5] N. M. L. Tan, T. Abe, and H. Akagi, "Design and performance of a bidirectional isolated dc–dc converter for a battery energy storage system," *IEEE Trans. Power Electron.*, vol. 27, no. 3, pp. 1237–1248, Mar. 2012.

[6] X. She, A. Q. Huang, S. Lukic, and M. E. Baran, "On integration of solid state transformer with zonal dc microgrid," *IEEE Trans. Smart Grid*, vol. 2, no. 3, pp. 975–985, Jun. 2012.

[7] K. Wang, C. Y. Lin, L. Zhu, D. Qu, F. C. Lee, and J. S. Lai, "Bi-directional dc/dc converters for fuel cell systems," in *Proc. IEEE Trans. Power Electron.*, Oct. 1998, pp. 47–51.

[8] F. Z. Peng, H. Li, G.-J. Su, and J. S. Lawler, "A new ZVS bidirectional dc–dc converter for fuel cell and battery application," *IEEE Trans. Power Electron.*, vol. 19, no. 1, pp. 54–65, Jan. 2004.

[9] L. Zhu, "A novel soft-commutating isolated boost full-bridge ZVS PWM dc–dc converter for bidirectional high power applications," *IEEE Trans. Power Electron.*, vol. 21, no. 2, pp. 422–429, Mar. 2006.

[10] D. P. Urciuoli and C. W. Tipton, "Development of a 90 kW bidirectional dc–dc converter for power dense applications," in *Proc. IEEE Appl. Power Electron. Conf.*, 2006, pp. 1375–378.

[11] J. Lee, J. Jo, S. Choi, and S.-B Han, "A 10-kW SOFC low-voltage battery hybrid power conditioning system for residential use," *IEEE Trans. Energy Convers.*, vol. 21, no. 2, pp. 575–585, Jun. 2006.

[12] G. Ma, W. Qu, G. Yu, Y. Liu, N. Liang, and W. Li, "A zero-voltage switching bidirectional dc–dc converter with state analysis and soft switching-oriented design consideration," *IEEE Trans. Ind. Electron.*, vol. 56, no. 6, pp. 2174–2184, Jun. 2009.

[13] Y. Du, X. Zhou, S. Bai, S. Lukic, and A. Huang, "Review of non-isolated bidirectional dc–dc converters for plug-in hybrid electric vehicle charge station application at municipal parking decks," in *Proc. IEEE Appl. Power Electron. Conf.*, 2010, pp. 1145–1151.

[14] M. H. Kheraluwala, R. W. Gascoigne, D. M. Divan, and E. D. Baumann, "A three-phase soft-switched high-power-density dc/dc converter for high-power application," *IEEE Trans. Ind. Appl.*, vol. 27, no. 1, pp. 63–73, Jan./Feb. 1991.

[15] M. N. Kheraluwala, R. W. Gascoigne, D. M. Divan, and E. D. Baumann, "Performance characterization of a high-power dual active bridge dc-to-dc converter," *IEEE Trans. Ind. Appl.*, vol. 28, no. 6, pp. 1294–1301, Dec. 1992.

[16] F. Krismer, S. Round, and J. W. Kolar, "Performance optimization of a high current dual active bridge with a wide operating voltage range," in *Proc. IEEE Power Electron. Spec. Conf.*, 2006, pp. 1–7.

[17] F. Krismer and J. W. Kolar, "Accurate small-signal model for the digital control of an automotive bidirectional dual active bridge," *IEEE Trans. Power Electron.*, vol. 24, no. 12, pp. 2756–2768, Dec. 2009.

[18] S. Inoue and H. Akagi, "A bidirectional dc–dc converter for an energy storage system with galvanic isolation," *IEEE Trans. Power Electron.*, vol. 22, no. 6, pp. 2299–2306, Nov. 2007.

[19] F. Krismer and J. W. Kolar, "Accurate power loss model derivation of a high-current dual active bridge converter for an automotive application," *IEEE Trans. Power Electron.*, vol. 57, no. 3, pp. 881–891, Mar. 2010.

[20] C. Leung, S. Dutta, S. Baek, and S. Bhattacharya, "Design considerations of high-voltage and high-frequency three-phase transformer for solid state transformer application," in *Proc. IEEE Energy Convers. Congr. Expo.*, 2010, pp. 1551–1558.

[21] J. Zhang, F. Zhang, X. Xie, D. Jiao, and Z. Qian, "A novel ZVS dc/dc converter for high-power applications," *IEEE Trans. Power Electron.*, vol. 19, no. 2, pp. 420–429, Mar. 2004.

[22] H. Bai and C. Mi, "Eliminate reactive power and increase system efficiency of isolated bidirectional dual-active-bridge dc–dc converter using novel dual-phase-shift control," *IEEE Trans. Power Electron.*, vol. 23, no. 6, pp. 2905–2914, Nov. 2008.

[23] G. G. Oggier, G. O. García, and A. R. Oliva, "Switching control strategy to minimize dual active bridge converter losses," *IEEE Trans. Power Electron.*, vol. 24, no. 7, pp. 1826–1838, Jul. 2009.

[24] G. G. Oggier, G. O. Garcíia, and A. R. Oliva, "Modulation strategy to operate the dual active bridge dc–dc converter under soft-switching in the whole operating range," *IEEE Trans. Power Electron.*, vol. 26, no. 4, pp. 1228–1236, Apr. 2011.

[25] B. Zhao, Q. Yu, and W. Sun, "Extended-phase-shift control of isolated bidirectional dc–dc converter for power distribution in microgrid," *IEEE Trans. Power Electron.*, vol. 27, no. 11, pp. 4667–4680, Nov. 2012.

[26] G. Ortiz, J. Biela, D. Bortis, and J. W. Kolar, "1 Megawatt, 20 kHz, isolated, bidirectional 12 kV to 1.2 kV dc–dc converter for renewable energy applications," in *Proc. Int. Power Electron. Conf.*, 2010, pp. 3212–3219.

[27] X. Li and A. K. Bhat, "Analysis and design of high-frequency isolated dual-bridge series resonant dc/dc converter," *IEEE Trans. Power Electron.*, vol. 25, no. 4, pp. 850–862, Apr. 2010.

[28] Y. Du, X. Bian, S. Lukic, B. S. Jacobson, and A. Q. Huang, "A novel wide voltage range bi-directional series resonant converter with clamped capacitor voltage," in *Proc. IEEE Ind. Electron. Soc.*, 2009, pp. 82–87.

[29] R. P. Severns, "Topologies for three-element resonant converters," *IEEE Trans. Power Electron.*, vol. 7, no. 1, pp. 89–98, Jan. 1992.

[30] X. Fang, H. Hu, Z. J. Shen, and I. Batarseh, "Operation mode analysis and peak gain approximation of the LLC resonant converter," *IEEE Trans. Power Electron.*, vol. 27, no. 4, pp. 1985–1995, Apr. 2012.

[31] R. Beiranvand, B. Rashidian, M. R. Zolghadri, and S. M. Hossein Alavi, "A design procedure for optimizing the LLC resonant converter as a wide output range voltage source," *IEEE Trans. Power Electron.*, vol. 27, no. 8, pp. 3749–3763, Aug. 2012.

[32] W. Feng, F. C. Lee, and P. Mattavelli, "Optimal trajectory control of burst mode for LLC resonant converter," *IEEE Trans. Power Electron.*, vol. 28, no. 1, pp. 457–466, Jan. 2013.

[33] G. Pledl, M. Tauer, and D. Buecherl, "Theory of operation, design procedure and simulation of a bidirectional LLC resonant converter for

vehicular applications," in *Proc. IEEE Vehicle Power Propulsion Conf.*, 2010, pp. 1–5.
[34] J.-H. Jung, H.-S. Kim, J.-H. Kim, M.-H. Ryu, and J.-W. Baek, "Design methodology of bidirectional CLLC resonant converter for high-frequency isolation of dc distribution systems," *IEEE Trans. Power Electron.*, vol. 28, no. 4, pp. 1741–1755, Apr. 2013.
[35] T. Jiang, J. Zhang, X. Chen, and Y Wang, "Bidirectional LLC resonant converter for energy storage applications," in *Proc. IEEE Appl. Power Electron. Conf.*, 2013, pp. 1145–1151.
[36] G. Ivensky, S. Bronshtein, and A. Abramovitz, "Approximate analysis of resonant LLC dc–dc converter," *IEEE Trans. Power Electron.*, vol. 26, no. 11, pp. 3274–3284, Nov. 2011.

Tianyang Jiang was born in Liaoning, China, in 1987. He received the B.S. degree in electrical engineering from Zhejiang University, Hangzhou, China, in 2010, where he is currently working toward the Ph.D. degree in electrical engineering.

His current research interests include power electronics system integrations and high-efficiency converters.

Junming Zhang (M'10–SM'13) received the B.S., M.S., and Ph.D. degrees from Zhejiang University, Hangzhou, China, in 1996, 2000, and 2004, respectively, all in electrical engineering.

He is currently a Professor at the College of Electrical Engineering, Zhejiang University. From 2010 to 2011, he was a Visiting Scholar in the Department of Electrical and Computer Engineering, Michigan State University, East Lansing, MI, USA. His research interests include power electronics system integrations, power management, and high-efficiency converters.

Xinke Wu (M'10) received the B.S degree and M.S degree in electrical engineering from Harbin Institute of Technology, Harbin, China, in 2000 and 2002, respectively, and received the Ph.D. degree in electrical engineering from Zhejiang University, Hangzhou, China in 2006.

He was a Postdoctoral Fellow of National Engineering Research Center for Applied Power Electronics, Zhejiang University from 2007 to 2009, and was an Assistant Research Fellow from 2009 to 2010. From 2011 to 2012, he was a Visiting Scholar in Center of Power Electronics System, Virginia Polytechnic Institute and State University, Blacksburg, VA, USA. Since 2011, he has been an Associate Professor in electrical engineering with Zhejiang University. His research covers high-efficiency LED driving technology, soft switching, and high-efficiency power conversion, and power electronics system integration.

Dr. Wu was awarded as Distinguished Young Scholar of Zhejiang University in 2012.

Kuang Sheng (M'99–SM'08) received the B.S. degree in electrical engineering from Zhejiang University, Hangzhou, China, in 1995, and the Ph.D. degree in electrical engineering from Heriot-Watt University, Edinburgh, U.K., in 1999.

He has a Postdoctoral Research Associate at Cambridge University, Cambridge, U.K., between 1999 and 2002. He was at Rutgers University, New Brunswick, NJ, USA, where he was an Assistant Professor and a tenured Professor from 2002 to 2009. He led a team that reported the first power IC on SiC. He is currently at Zhejiang University as a tenured Professor. He has published approximately 90 technical papers in international journals and conferences and holds 12 patents. His research interests include all aspects of power semiconductor devices and ICs on SiC and Si.

Dr. Sheng serves as an Associate Editor of the IEEE TRANSACTIONS ON POWER ELECTRONICS and the IEEE TRANSACTIONS ON INDUSTRIAL APPLICATIONS.

Yousheng Wang received the B.S. degree from the Department of Electrical Engineering, Zhejiang University, Hangzhou, China.

He became a Professor in 1978. His research interests include power electronics and high-frequency induction heating.

Mr. Wang received several national awards for his outstanding works in large electric generator and static induction heating equipment. He is a Member of the China Academy of Engineering.